Korean Journal of Remote Sensing, Vol.24, No.5, 2008, pp.483~496

Validation and selection of GCPs obtained from ERS SAR and the SRTM DEM: Application to SPOT DEM Construction

Hyung-Sup Jung, Sang-Hoon Hong, and Joong-Sun Won †

Department of Earth System Sciences, Yonsei University, 134 Shinchon-dong, Seodaemun-gu, Seoul 120-749, Korea

Abstract : Qualified ground control points (GCPs) are required to construct a digital elevation model (DEM) from a pushbroom stereo pair. An inverse geolocation algorithm for extracting GCPs from ERS SAR data and the SRTM DEM was recently developed. However, not all GCPs established by this method are accurate enough for direct application to the geometric correction of pushbroom images such as SPOT, IRS, etc, and thus a method for selecting and removing inaccurate points from the sets of GCPs is needed. In this study, we propose a method for evaluating GCP accuracy and winnowing sets of GCPs through orientation modeling of pushbroom image and validate performance of this method using SPOT stereo pair of Daejon City. It has been found that the statistical distribution of GCP positional errors is approximately Gaussian without bias, and that the residual errors estimated by orientation modeling have a linear relationship with the positional errors. Inaccurate GCPs have large positional errors and can be iteratively eliminated by thresholding the residual errors. Forty-one GCPs were initially extracted for the test, with mean the positional error values of 25.6 m, 2.5 m and -6.1 m in the X-, Y- and Z-directions, respectively, and standard deviations of 62.4 m, 37.6 m and 15.0 m. Twenty-one GCPs were eliminated by the proposed method, resulting in the standard deviations of the positional errors of the 20 final GCPs being reduced to 13.9 m, 8.5 m and 7.5 m in the X-, Y- and Z-directions, respectively. Orientation modeling of the SPOT stereo pair was performed using the 20 GCPs, and the model was checked against 15 map-based points. The root mean square errors (RMSEs) of the model were 10.4 m, 7.1 m and 12.1 m in X-, Y- and Z-directions, respectively. A SPOT DEM with a 20 m ground resolution was successfully constructed using a automatic matching procedure.

Key Words : Qualified GCP, SPOT DEM, inverse geolocation algorithm, ERS SAR, SRTM DEM.

1. Introduction

Digital elevation models (DEMs) are required for many applications, such as watershed and groundwater monitoring, landslide forecasting, flood area mapping, land subsidence measurement, etc. Various remote sensing data and techniques have been used to construct DEMs, which include stereo-mapping (Raillou and Gelautz, 1999), LIDAR techniques (Lee and Younan, 2003), and radar interferometry (Rufino *et al.*, 1998). The Shuttle Radar Topography Mission (SRTM) was carried out to produce a global DEM for

Received October 1, 2008; Revised October 12, 2008; Accepted October 20, 2008.

† Corresponding Author: Joong-Sun Won (jswon@yonsei.ac.kr)

the region between the latitudes of N 60° and S 56° (Rabus *et al.*, 2003). The SRTM DEM was released at a spacing of 1 arc second (about 30 m) for the Unites States and at a spacing of 3 arc seconds (about 90 m) in the other regions. Despite the existence of a global DEM, DEMs of lesser extents and higher resolutions are often required for a multitude of applications. To fill this requirement, DEMs with a scale of 1:50,000 are often produced by stereo-mapping SPOT image pairs (Chen and Rau, 1993). However, since SPOT satellites have inaccurate orbit information, the generation of SPOT DEMs is contingent upon image rectification based on accurate ground control points (GCPs). The ground coordinates of GCPs can be established through field surveys or can be extracted from published maps. For many regions of the world, however, fine scale maps are not available and field surveys are not always possible. In such cases, the ground coordinates of the selected GCPs can be estimated from remotely sensed data with highly accurate orbit information.

Hong *et al.* (2006) recently proposed a rigorous method for extracting GCPs from ERS SAR data and the SRTM DEM. In their method, the SRTM DEM was used to generate a simulated SAR image for correcting the system timing errors and topographic effects of ERS SAR data. Each GCP was then calculated by an inverse geolocation approach. Although the method greatly improves the overall positional accuracy of the GCPs, it has the disadvantage of potentially including some GCPs with large positional errors. In such cases, the established GCPs do not maintain the overall positional accuracy adequate for pushbroom stereo pair development. Thus, to overcome this disadvantage, it became necessary to distinguish accurate and unqualified GCPs.

The objective of this study is to develop a high resolution DEM using a SPOT stereo pair rectified with qualified GCPs extracted from ERS SAR data and the SRTM DEM for a region where GCPs extracted from either a published map or a field survey are not available. The proposed method is contingent on the extracted GCPs having an approximately Gaussian distribution and on their residual errors, as obtained through orientation modeling, being proportional to their positional errors. Inaccurate GCPs are removed with respect to residual errors of orientation model ('residual errors' hereafter), and accurate GCPs are used to produce a DEM with a ground resolution of 20m. The accuracy of the extracted GCPs was evaluated against 1:5,000 national digital maps.

The following sections briefly describe the methods for extracting GCPs from ERS SAR data and the SRTM DEM. Also discussed is the relationship between positional errors of the GCPs and residual errors of the SPOT stereo pair's orientation model. The proposed method for eliminating inaccurate GCPs with residual errors is detailed, and a comparison of the SPOT stereo-based DEM and the SRTM DEM is offered.

2. Methodology

Following methods detailed by Hong *et al.* (2006), ground coordinates of GCPs identified in both SAR and SPOT images can be calculated using SAR geometry and the SRTM DEM. GCPs in SAR image space can be converted into ground space using the SRTM DEM, but a rigorous geometric relationship between the SAR image and ground spaces must first be defined. Inverse geolocation of the ERS SAR image is conducted by using the precise Delft orbit and a simulated SAR image generated from the SRTM DEM.

Fig. 1 shows the processing required to construct a

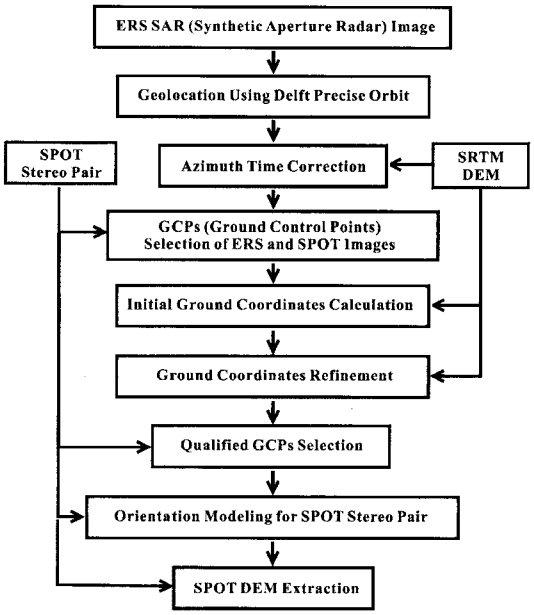

Fig. 1. The proposed flow of processing for GCP selection and SPOT DEM construction.

DEM from a SPOT stereo pair and the extracted GCPs. Each GCP in image coordinates (line, pixel) is selected as an identifiable pixel both in ERS SAR and SPOT images first. The ground coordinates (X, Y, Z) of each GCP are calculated by considering the geometries of the geolocated SAR image and the SRTM DEM. The collection of GCPs obtained via the aforementioned steps included inaccurate points, and thus did not meet the required accuracy of less than one SPOT image pixel. To evaluate GCP accuracy, an orientation model of the SPOT stereo pair is applied to the extracted GCPs. Inaccurate GCPs are iteratively eliminated through a thresholding process, where points are eliminated if they are more than two times the standard deviation of the residual errors of the model. The exterior orientation parameters, including the position and altitude angle of the satellite, are calculated with the qualified GCPs. To minimize the ambiguities in matching and improve computational efficiency, the rectified images are generated from SPOT stereo pair using the Earth ellipsoid equation, and image pyramids are formed by smoothing and subsampling of the rectified images. Finally, SPOT DEM is constructed by automatic matching process using the rectified images.

1) Inverse geolocation of SAR data and GCP extraction

The geometric relationship between ground coordinates representing earth surface position and the SAR image coordinates can be expressed by the Doppler and range equations, two basic SAR mapping equations (Curlander and McDough, 1991; Raillou and Gelautz, 1999). The Doppler and range equations are given by:

$$f_D(t) = \frac{2}{\lambda R(t)}(\vec{V}_S(t) - \vec{V}_T(t)) \cdot (\vec{P}_S(t) - \vec{P}_T(t)) \quad (1)$$

$$R(t) = |\vec{P}_S(t) - \vec{P}_T(t)| \quad (2)$$

where, t is a pixel-imaging time, f_D is Doppler frequency shift, λ is radar wavelength, $\vec{V}_S$ and $\vec{V}_T$ are satellite and target velocity vectors, respectively, $\vec{R}_S$ and $\vec{R}_T$ are satellite and target position vectors, respectively, the slant range distance R is the distance between satellite and target positions.

These equations can be used with the Earth ellipsoid equation to project image coordinates (line, pixel) into the ground coordinates (X, Y, Z) (Olmster, 1993). However, this approach cannot avoid positional errors because it assumes the Earth' s surface to be an ellipsoid. On the contrary, ground coordinates can be inversely mapped into image coordinates by the inverse geolocation algorithm (Olmster, 1993; Hong *et al.*, 2006). Hong *et al.* (2006) recently proposed such a sophisticated geolocation algorithm to successfully extract GCPs using ERS SAR data and the SRTM DEM. This algorithm is based on the relationship between the Doppler frequency shift and the Doppler centroid (f_{DC}), as given by:

$$f_D(t)-f_{DC}=\frac{2}{\lambda R(t)}(\vec{V}_S(t)-\vec{V}_T(t))\cdot(\vec{P}_S(t)-\vec{P}_T(t))-f_{DC}=0 \quad (3)$$

If the imaging time t is determined, the SAR image coordinates (line, pixel) can easily be estimated from the relationship between the imaging time and it (Olmster, 1993). The SRTM DEM is used for $\vec{R}_T$ values in Eq. (3). The algorithm proposed by Hong *et al.* (2006) is processed by three steps: 1) azimuth time correction using the simulated SAR data, 2) the initial ground coordinates estimation for SAR image coordinates with the Earth ellipsoid equation and Eq. (3), and 3) the refinement of the initial ground coordinates by the iterative process.

When a GCP candidate is selected, the object must be identified in both SAR and SPOT images. It is often difficult to find the conjugate points on both SAR and optic images due to differences in geometric and radiometric properties. It is, however, never impossible to find such GCPs (Toutin, 2000). Toutin *et al.* (1998) reported that conjugate points can be selected from SAR and optic images, even for areas with mountainous topography. In addition to visual selection method, co-registration of SAR and optic images has been conducted using interferometric phase (Raucoules and Carnec, 1999) and automatic feature-based registration (Dare and Dowman, 2001).

In this study, GCP candidates are selected from ERS SAR data and a SPOT stereo pair. The inverse geolocation algorithm is then used to calculate GCP ground coordinates from ERS SAR image coordinates and SRTM DEM ground coordinates.

2) Orientation modeling for SPOT stereo pair

The collinearity condition states that the exposure station and any ground point and its image point together lie along a straight line, and the condition is applied to satisfy optic image geometry. The collinearity equations for SPOT images are defined as (Chen and Rau, 1993; Orun and Natarajan, 1994):

$$x_i=-f\frac{m_{11}\cdot(X_i-X_s(t))+m_{12}\cdot(Y_i-Y_s(t))+m_{13}\cdot(Z_i-Z_s(t))}{m_{31}\cdot(X_i-X_s(t))+m_{32}\cdot(Y_i-Y_s(t))+m_{33}\cdot(Z_i-Z_s(t))} \text{ and} \quad (4)$$

$$y_i=-f\frac{m_{21}\cdot(X_i-X_s(t))+m_{22}\cdot(Y_i-Y_s(t))+m_{33}\cdot(Z_i-Z_s(t))}{m_{31}\cdot(X_i-X_s(t))+m_{32}\cdot(Y_i-Y_s(t))+m_{33}\cdot(Z_i-Z_s(t))}, \quad (5)$$

where f is the focal length, x_i and y_i are the image coordinates, X_i, Y_i and Z_i are the ground coordinates of the ith point, X_s, Y_s and Z_s are the satellite position, and m_{11}, m_{12}, $\cdots$, and m_{33} are elements of the rotation matrix defined by the satellite attitude, which is formed by the roll angle (ω), the pitch angle (φ) and the yaw angle (k).

The exterior orientation parameters, including the satellite position and the yaw angle of the satellite, are characterized by second order polynomials as functions of time (Orun and Natarajan, 1994). The roll and pitch angles are excluded from the exterior orientation parameters because they are indistinguishable from X_s and Y_s components of satellite position (Orun and Natarajan, 1994). These parameters are determined and refined using GCPs. This procedure comprises a space resection, which is applied individually to each optic image of a stereo pair, and a space intersection that generates the ground coordinates of GCPs measured on the images. It is generally supposed that GCPs in orientation modeling are free of positional error, and such an assumption might be true for GCPs read from a published map. However, the innate positional errors of GCPs extracted from ERS SAR data and the SRTM DEM seriously affect orientation modeling results.

Provided that GCPs are corrupted by positional errors, and that their positional errors are random and maintain a Gaussian distribution with a zero mean, positional errors will be proportional to the residual errors of the orientation model. This is because the exterior orientation parameters are determined by a least mean square estimation, which results in

residual errors of less accurate GCPs being larger than those of accurate GCPs. Although the adopted assumptions are not always satisfactory for extracted GCPs, the relationship between residual and positional errors should be preserved when the magnitude of positional error exceeds that of other errors. For this reason, the quality of extracted GCPs can be evaluated based on the residual errors of the orientation model. However, the application of such evaluation techniques is constrained by the uncertain linear relationship between positional and residual errors, because positional errors of extracted GCPs have not exactly a Gaussian distribution. This constraint can be easily overcome through an iterative procedure. All of the GCPs are used to develop the first orientation model of the SPOT stereo pair. Severely inaccurate GCPs are identified by thresholding the residual errors that exceed a predetermined value, herein established as two times the standard deviation (i.e. 95.4% confidence level) of the residual errors. Orientation modeling is iteratively conducted using only survived GCPs with an updated standard deviation until the residual errors of the remaining GCPs are all lower than the threshold. Section 4 shows that inaccurate GCPs are efficiently eliminated by the proposed method.

3) DEM extraction

DEM extraction requires stereo image matching. Image matching is an intrinsically difficult problem, because ambiguous matches exist for most features. To minimize the ambiguities in matching and improve computational efficiency, the matching algorithm used proceeds using rectified images and image pyramids. The rectified images are generated from the SPOT stereo pair using Eqs. (4) and (5) and the Earth ellipsoid equation with the mean height of AOI (area of interest). To search matching points fast and exactly, the multiple resolution image pyramids are generated by smoothing and subsampling of the rectified image. The disparity map at lowest resolution images is firstly obtained from area matching, and used to guide matching at next resolution level. This process continues until the final area matching is performed at full resolution (Mikhail *et al.*, 2001). Ground coordinates are then calculated from the refined set of conjugate points of the resulting disparity map using Eq. (4) and (5), and a 20 m DEM is finally interpolated in grid format by Kriging.

3. Study area and dataset

The study area is in Daejon City, Korea, an area consisting of steep mountains, lakes, and city infrastructure including buildings, roads, bridges, etc. ERS-1 SAR data were acquired on 22 December 1995 by a descending path with a viewing angle of 23 degrees. The nominal sampling space of the ERS-1 SAR single-look-complex (SLC) data were 5 m and 10 m in azimuth and range, respectively. The images composing the SPOT-3 stereo pair were acquired on 4 April 1995 and 4 March 1995 at viewing angles of -22.7 and 8.6 degrees, respectively. The SPOT-3 images had a nominal ground resolution of 10 m in both lines and pixels. The SRTM DEM is provided by the United States Geological Survey, has a grid spacing of 3 arc seconds in the study area, and has planimetric and height accuracies of 60 m and 16 m in, respectively (Marschalk *et al.*, 2004). National digital 1:5,000 maps with planimetric and height accuracies of about 2 m, were used to evaluate the accuracy of the extracted GCPs. The accuracy of orientation modeling results was evaluated using 15 check points read from the national digital maps.

A SAR image was simulated with the SRTM DEM and a precise Delft orbit provided by DEOS. The Delft orbit maintains a precision of up to 5 cm

when solar activity is very low (Remko and Pieter, 1998). An amplitude SAR image was generated from ERS-1 SAR SLC data so that conjugate points could be identified in the ERS SAR image. A 5 by 5 gamma filter (Lopes *et al.*, 1993) was then applied to the amplitude SAR image to reduce speckle noise. A 95% linear histogram stretch was applied to the SPOT amplitude images to improve visual perceptibility.

4. Results

A total of 41 GCP candidates were selected and applied to the orientation model of the SPOT stereo pair to eliminate inaccurate GCPs. Twenty qualified GCPs survived the elimination process. Orientation modeling of the SPOT stereo pair was successfully conducted using the 20 quialfied GCPs, and a qualified DEM was constructed from the SPOT stereo pair. The result was verified using 15 check points extracted from a 1:5,000 national digital map.

1) Validation of GCPs for the SPOT stereo pair

A total of 41 conjugate points were selected as initial GCP candidates from the ERS SAR image and SPOT stereo pair. The spatial distribution of the 41 original GCP candidates and 15 check points is shown in Fig. 2. These GCPs were identified at crossroads, lake edges, bridges, landmark buildings, etc. As the study area included portions of a city, crossroads were easily identified both in ERS SAR and SPOT images. In the SAR image, roads were characterized by low brightness because of their specular surface, and buildings adjacent to roads were easily characterized by bright corners. Such contrasting characterizations made urban crossroads easily identifiable in the SAR image, but the identification of GCPs was difficult in the areas

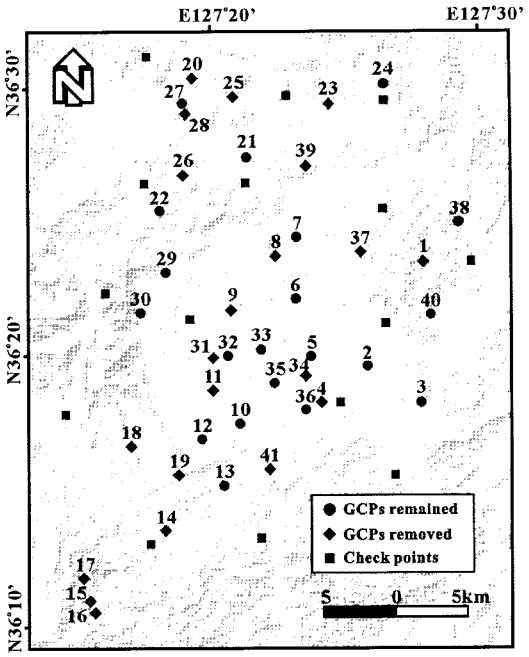

Fig. 2. Distribution of the 41 GCP candidates and the 15 check points (denoted by square). The eliminated and maintained GCPs are denoted by diamonds and solid circles, respectively.

lacking artificial features. The edges of water bodies served as good identifiers in suburban and rural areas because the backscattering from smooth water surfaces was low relative to that from the surfaces surrounding water bodies. Fig. 3 shows an example GCP that corresponds to an easily identifiable crossroad.

As described in the Section 2.1, the ground coordinates of the GCP candidates were calculated by applying the inverse geolocation method to ERS SAR data and the SRTM DEM. The accuracy of each GCP was estimated using reference data and the 1:5,000 national digital map. The GCP accuracies are presented in Table 1. Similar to the result reported by Hong *et al.* (2006), the overall GCP accuracy was not adequate for SPOT image rectification when all 41 GCPs were used. Table 2 summarizes error statistics of the 41 GCP candidates. Maximum errors in the X-, Y- and Z-directions were 296.9 m, -162.8m and -76.8 m, respectively. Mean values of the positional errors

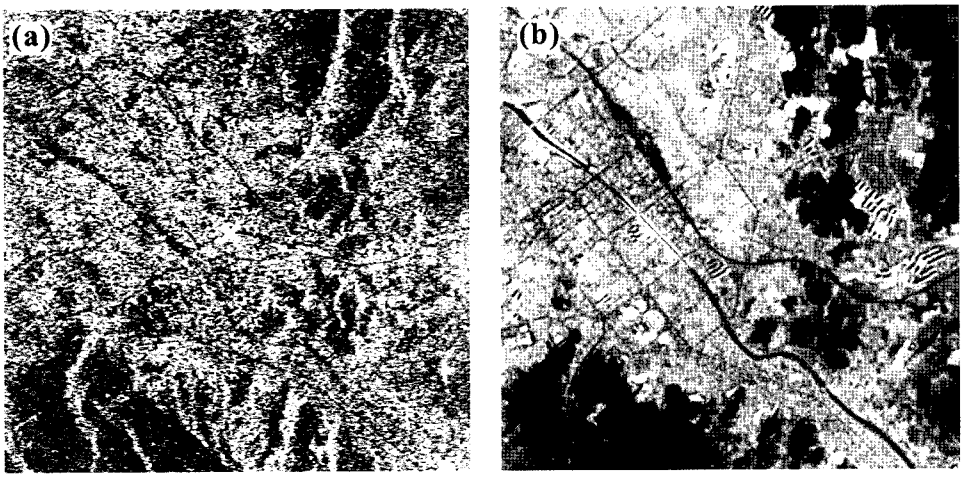

Fig. 3. (a) ERS SAR and (b) SPOT images. Crossroads are here shown to be good candidates for GCP identification.

Table 1. Positional errors of GCPs extracted from ERS SAR data and the SRTM DEM. The positional errors were estimated using a 1:5,000 national digital map.

ID	Positional errors			Qualified GCPs*	ID	Positional errors			Qualified GCPs*
	X (m)	Y (m)	Z (m)			X (m)	Y (m)	Z (m)	
1	57.3	11.6	7.7	X	22	27.7	12.9	1.1	X
2	**8.8**	**0.0**	**-5.4**	**O**	23	-3.7	13.8	-6.2	X
3	**0.9**	**1.9**	**-14.4**	**O**	**24**	**-13.1**	**-3.5**	**-0.5**	**O**
4	46.8	42.3	0.1	X	25	36.7	-6.9	-7.4	X
5	**-16.6**	**4.2**	**-7.0**	**O**	26	41.0	17.7	-0.9	X
6	**12.1**	**9.6**	**6.9**	**O**	**27**	**20.6**	**23.6**	**2.1**	**O**
7	**-3.0**	**11.5**	**1.8**	**O**	28	-9.5	-81.2	-0.1	X
8	63.5	50.8	-4.4	X	**29**	**22.2**	**7.8**	**-21.9**	**O**
9	-21.8	11.1	0.1	X	**30**	**31.5**	**0.2**	**-8.0**	**O**
10	**1.8**	**4.8**	**6.8**	**O**	31	15.0	-35.2	11.3	X
11	45.9	-1.0	-3.6	X	**32**	**-6.7**	**15.0**	**0.8**	**O**
12	**7.1**	**0.2**	**-1.5**	**O**	**33**	**16.7**	**-1.8**	**-8.4**	**O**
13	**6.8**	**15.4**	**-9.1**	**O**	34	296.9	95.6	-3.2	X
14	113.4	3.5	-47.3	X	**35**	**7.6**	**16.7**	**-2.2**	**O**
15	152.7	-23.7	-76.8	X	**36**	**-4.1**	**14.9**	**-11.6**	**O**
16	**-0.9**	**22.0**	**2.0**	**O**	37	17.7	-22.6	-21.8	X
17	3.7	11.3	-3.0	X	**38**	**22.4**	**8.9**	**7.4**	**O**
18	163.1	-34.7	-9.0	X	39	-39.2	11.3	2.7	X
19	-93.8	-162.8	-11.2	X	**40**	**29.6**	**-6.4**	**-9.1**	**O**
20	8.6	50.9	-1.1	X	41	-6.6	-15.6	-5.2	X
21	**-10.4**	**7.7**	**-1.7**	**O**					
Mean of 41 GCPs						25.6	2.5	-6.1	
Mean of selected 20 GCPs						6.7	7.6	-3.7	

* 'O' and 'X' represent qualified and disqualified GCPs, respectively.

were 25.6 m, 2.5 m and -6.1 m in X-, Y- and Z-directions, respectively, and standard deviations were 62.4 m,?37.6 m and 15.0 m. The overall accuracy in the Z-direction was better than the horizontal accuracies. The SRTM DEM maintains vertical and horizontal accuracies of 16 and 60 m, respectively (Marschalk *et al.*, 2004). This result implies that the accuracy of GCPs extracted from ERS SAR data and the SRTM DEM

Table 2. Positional error statistics of the 41 original GCP candidates extracted from SRTM elevation data and ERS SAR data.

Direction	Mean (m)	std. (σ) (m)	Negative Max. (m)	Positive Max. (m)
X	25.6	62.4	-93.8	296.9
Y	2.5	37.6	-162.8	95.6
Z	-6.1	15.0	-76.8	11.3

depends upon the accuracy of the SRTM DEM.

Accuracy of each GCP was evaluated against the residual error of the orientation model as explained in the Section 2.2. GCPs with a residual error of greater than two times the standard deviation (2σ) of the residual errors were discarded for being inaccurate. This procedure was conducted iteratively until the all remaining GCPs maintained a residual error less than 2σ. This iterative process resulted in the selection of twenty qualified GCPs (see Fig. 3 and Table 1).

Fig. 4 displays positional error histograms of the original 41 GCP candidates in three directions. In the plots, the error range is limited to between -100 m and +100 m, and errors larger than ± 100 m are represented at the end points. Four GCP candidates had X errors larger than +100 m, causing a positive shift of the mean error value. Exclusion of those four points reduced the mean error in X to 8.7 m. Using SPSS 13.0, the normality of positional errors was analyzed by the Shapiro-Wilk test (Shapiro and Wilk, 1965). This test provides evidence for certain types of "non-normality" if the P value is less than 0.05. P values of positional errors for the 41 GCP candidates were 0.000 in all directions, indicating that the positional errors did not fit a normal, Gaussian distribution. The normality of the positional errors was not satisfied in terms of Shapiro-Wilk test, but the non-normality was caused by a few points with large errors. With the removal of 5, 3, and 2 GCPs with large errors in the X-, Y- and Z-directions, the P values were greatly improved to be 0.815, 0.025 and 0.257, respectively.

The first iteration of the orientation model was constructed with all 41 GCPs. Fig. 5 shows the relationship between the positional errors and the residual errors obtained from the orientation model. The graphs in Fig. 5 (a) and (b) show that the positional errors are linearly proportional to the residual errors in the X- and Y-directions. The coefficients of determination, r^2, were 0.89 and 0.83 in X- and Y-directions, respectively. Therefore, it is reasonable to assume that residual errors of the orientation model maintain a linear relationship with the positional errors. If the GCPs used are free from positional errors, the residual errors of the orientation model should not be correlated with the positional errors. Thus, the linear relationship implied that

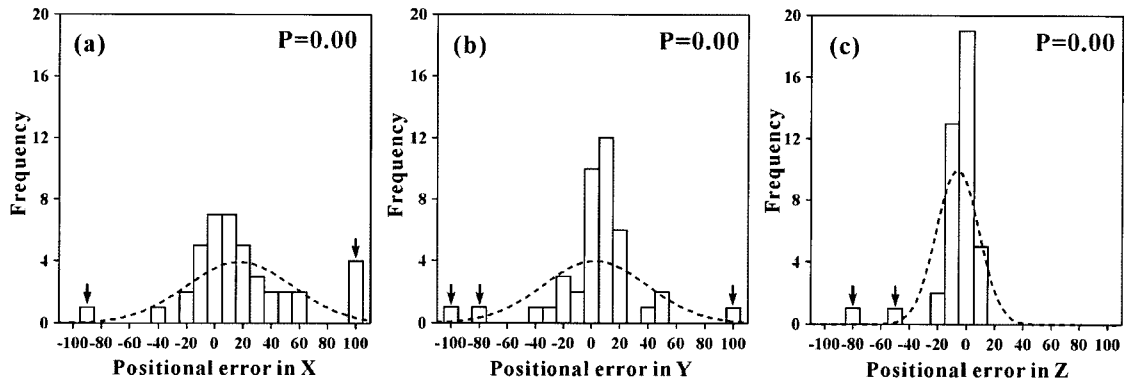

Fig. 4. Positional error histograms of the 41 GCP candidates. (a), (b) and (c) present positional errors in the X-, Y- and Z-directions, respectively. Positional errors were estimated using a 1:5,000 national digital map. Arrows denote errors identified as unusually large by the Shapiro-Wilk test.

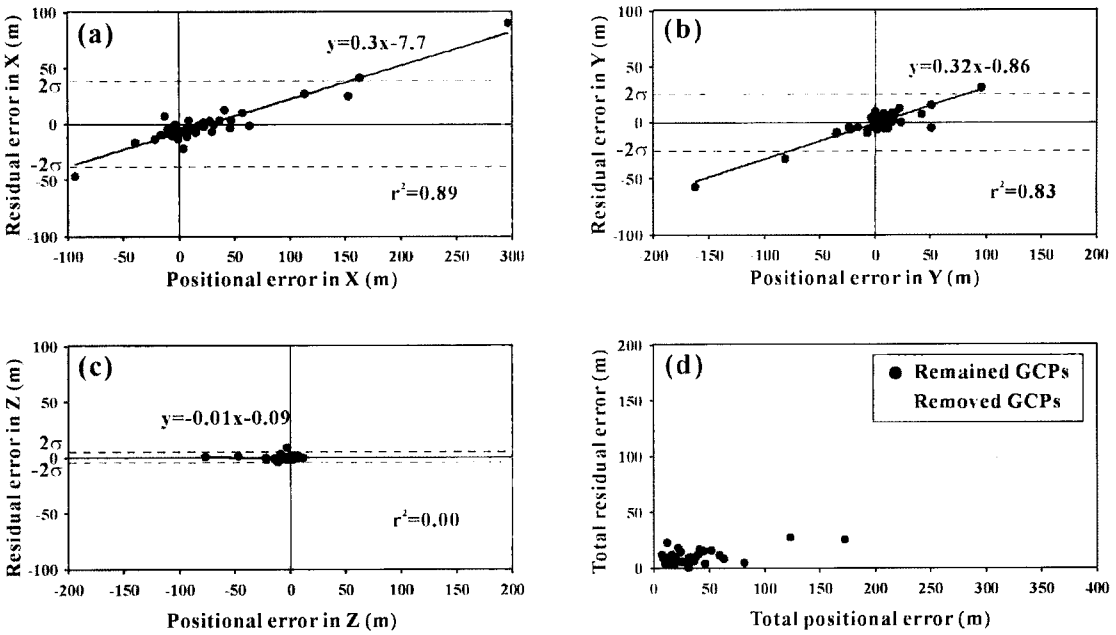

Fig. 5. Residual errors versus positional errors in the (a) X-, (b) Y-, and (c) Z-directions, as estimated through orientation modeling using the 41 GCP candidates. The dashed line represents the data range under 2σ (two times the standard deviation). (d) Total residual errors versus total positional errors.

positional error was larger than the other errors and that their distributions could be reasonably assumed to be Gaussian in the X- and Y-directions. Although the residual and positional errors maintained a linear relationship, their standard deviation was not identical. Positional errors in the Z-direction were independent of the residual errors ($r^2 = 0.00$) because the positional errors were relatively small and because errors in the Z-direction were sensitive to the selection of conjugate points for the stereo pair. Based on the linear relationship between residual and positional errors, GCPs with positional errors of larger than two times the standard deviation of the residual errors were considered to be inaccurate. In the first iteration, there were 3 inaccurate GCPs in X- and Y-directions and 1 inaccurate GCP in the Z-direction. Thus a total of 4 GCPs were identified as inaccurate and eliminated from the initial set of GCP candidates (Fig. 5(d)). Table 3 summarizes the standard deviation of residual errors and the number of eliminated GCPs candidates at each iteration. Standard deviations in first iteration were 19.9 m, 13.2 m and 1.8 m in X, Y and Z directions, respectively. The remaining 37 GCP candidates were used for the second iteration of orientation modeling, which maintained a coefficient of determination, r^2, of 0.73 in the X-direction. The correlation between

Table 3. The standard deviations (σ) of the residual errors of GCPs in the X-, Y- and Z-directions, as obtained through orientation modeling of the SPOT stereo pair. Also shown is the number of GCPs eliminated at each iteration.

No. of iteration	std. (σ) of residual errors			No. of eliminated GCPs
	X (m)	Y (m)	Z (m)	
1	19.9	13.2	1.8	4
2	9.3	5.4	0.6	7
3	5.2	3.6	0.5	3
4	3.3	3.2	0.4	3
5	2.9	2.6	0.5	1
6	3.0	2.3	0.4	2
7	2.9	1.8	0.4	1
8	2.9	1.6	0.3	0

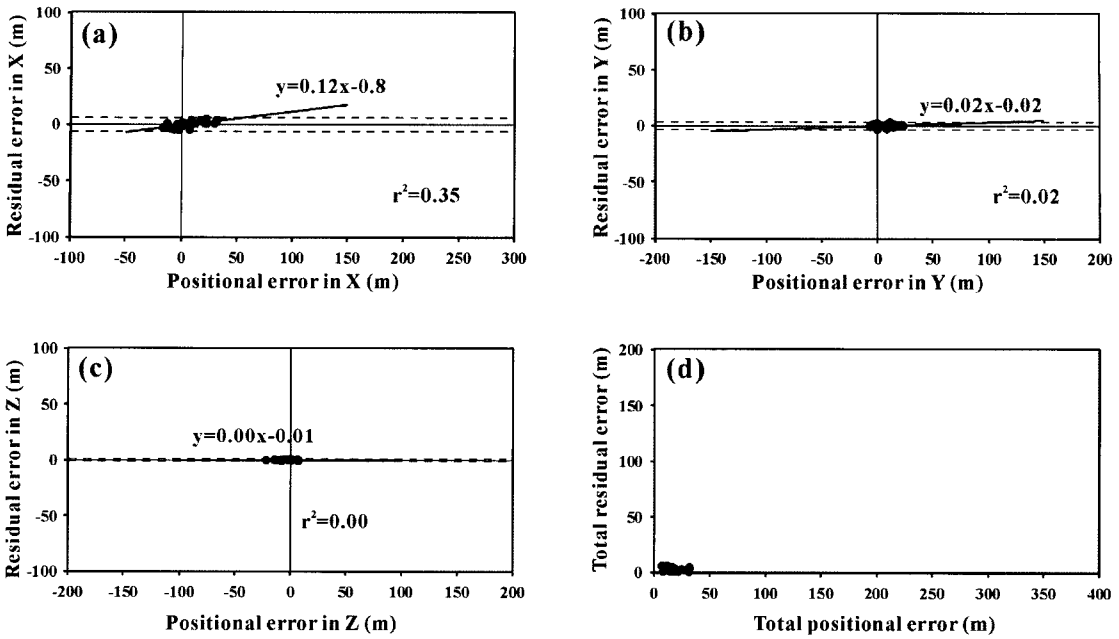

Fig. 6. Residual errors versus positional errors in the (a) X-, (b) Y-, and (c) Z-directions, estimated using the final 20 GCPs. The dashed line represents the data range under 2σ. (d) Total residual errors versus total positional errors.

the positional and residual errors was still high, but the r^2 in the Y-direction decreased to 0.37. This result indicates that the positional errors in the Y-direction were largely improved, but that errors were still large in the X-direction. Seven GCPs were eliminated in the second iteration. A total of eight iterations of orientation modeling were required to obtain a set of qualified GCPs. As shown in Table 3, standard deviations at the eighth iteration were reduced to small values due to the elimination of GCPs with larger positional errors.

As shown in Table 1, 21 of the 41 original GCPs were eliminated through iterative modeling. Fig. 6 displays the relationship between the positional and residual errors of the 20 final GCPs. In the Y-direction, the r^2 of the residual errors was 0.83 with 41 GCP candidates, but only 0.02 when only the 20 qualified GCPs were considered. The linear relationship between the positional and residual errors was also no longer significant in the Y-direction. The standard deviation of positional errors in the Y-direction was greatly reduced from 37.6 m to 8.5 m, meaning that the positional errors in the Y-direction were no longer a serious error component in the orientation model. The r^2 of the residual errors in the Z-direction was 0.00, which equals the r^2 of the 41 GCP candidates. However, the standard deviation in the Z-direction was reduced from 15.0 m to 7.5 m due to the elimination of the large positional errors of inaccurate GCPs. In the X-direction, the r^2 was still high at 0.35, and the positional errors were little improved relative to improvements in the in Y- and Z-directions. Thus, errors in the X-direction strongly influenced the residual errors, despite a reduction in their standard deviation from 62.4 m to 13.9 m. This result is confirmed in Fig. 7 by the positional error histograms of the 20 final GCPs. Relative to Fig. 4, the histograms shown in Fig. 7 more closely represent a true Gaussian distribution. P values of the Shapiro-Wilk test were 0.782, 0.732 and 0.497 in X-, Y- and Z-directions, respectively, and positional errors formed a normal distribution in all directions. The

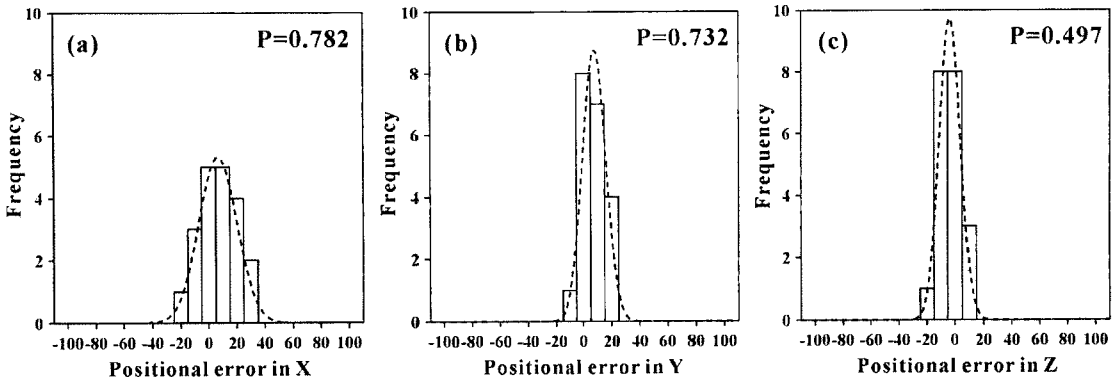

Fig. 7. Positional error histograms of the final 20 GCPs. (a), (b) and (c) present the positional errors in the X-, Y- and Z-directions, respectively.

Gaussian distributions in the Y- and Z-directions had higher and narrower peaks than in the X-direction, indicating that the positional errors in the X-direction were not properly reduced as in the other directions.

Fig. 8(a) depicts the residual error vectors of the initial 41 GCP candidates while Fig. 8(b) shows those of the 20 selected GCPs. The length of the error vector in Fig. 8 represents the values of residual errors, and the Figs prove the effectiveness of the proposed method. Fifteen check points (gray squares in Fig. 4) from the 1:5,000 digital map of the study area were used to validate orientation modeling results. As shown in Table 4, RMSEs estimated using the 15 check points were 10.4 m, 7.1 m, and 12.1 m

Table 4. Total directional RMSEs of the SPOT orientation model. The errors were estimated from 15 check points.

RMSEs (m)		
X	Y	Z
10.4	7.1	12.1

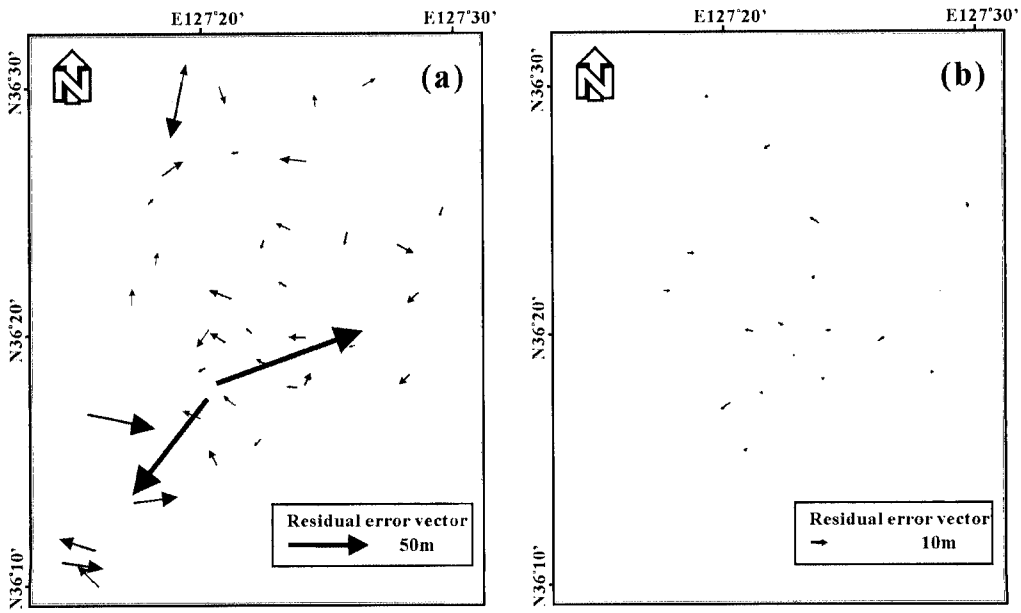

Fig. 8. Residual error vectors of the GCPs after orientation modeling for the SPOT stereo pair. The results are based on (a) the 41 initial GCP candidates and (b) the 20 GCPs finally selected.

in X-, Y-, and Z-directions, respectively. This accuracy was enough to construct a SPOT DEM grid with a resolution of 20 m. Thus, it is confirmed that GCP candidates with large positional errors can be effectively excluded using residual errors from orientation modeling, and a set of qualified GCPs may be used to georeference a SPOT stereo pair for DEM construction.

Although the proposed method is well suited for the selection of qualified GCPs, it does maintain some disadvantages. The proposed method successfully distinguishes qualified GCPs from GCP candidates extracted from the SRTM DEM and ERS SAR data. However, the process in the experiment discarded more than 50% of the originally extracted GCP candidates. Consequently, it may be ncessary to initially extract more than twice the minimum number of GCPs. The proposed method does not improve positional errors, but rather establishes a subset of qualified GCPs. Thus, if the majority of the

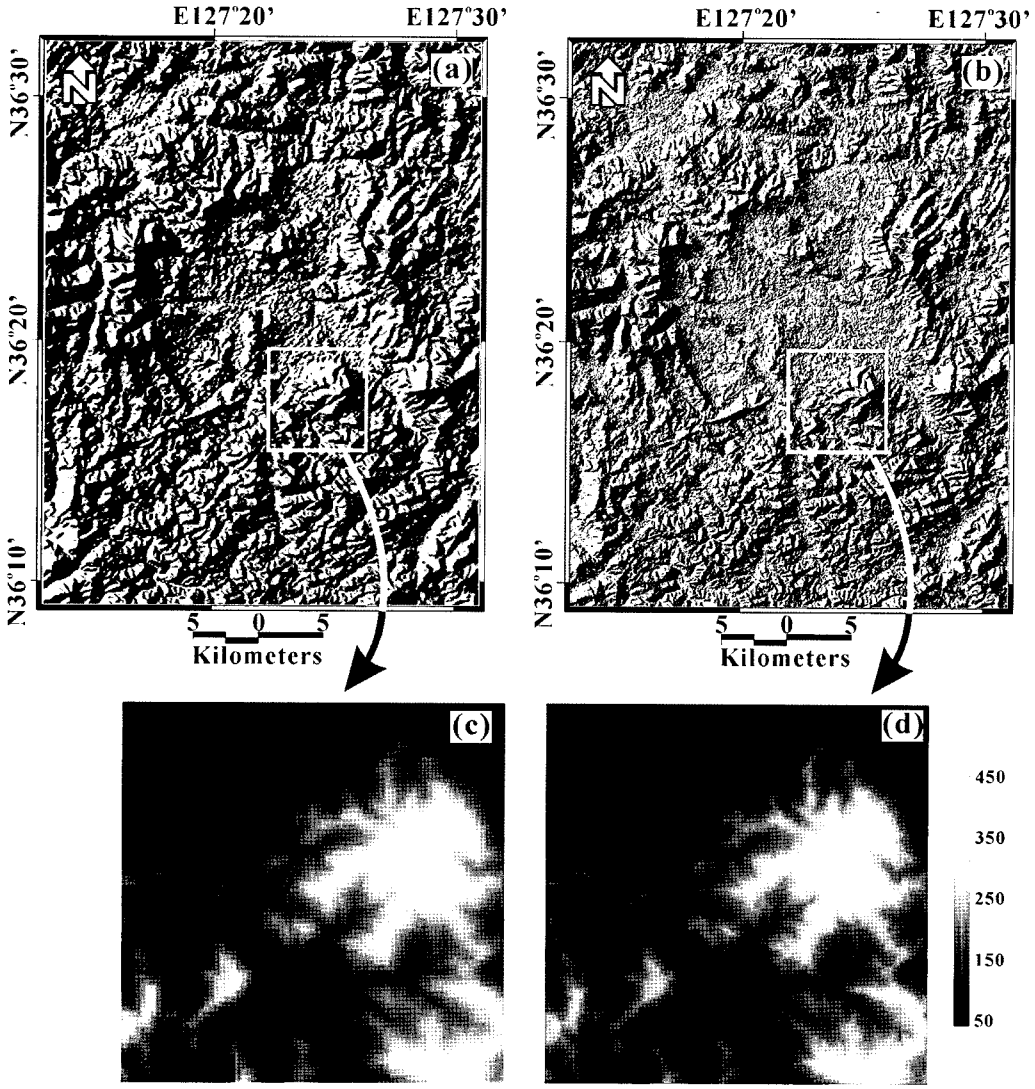

Fig. 9. Shadow relief maps of (a) SRTM elevation data and (b) the SPOT DEM constructed by the proposed method. (c) and (d) display grey-scale area maps encompassing the sub-selected areas presented in (a) and (b).

originally extracted GCPs are inaccurate, the proposed method should not be applied.

2) DEM accuracy assessment

Epipolar images were generated from the SPOT stereo pair using the 20 final GCPs, and 4 pyramid images were created by bi-cubic interpolation. Aerial based matching was first applied to the top-level pyramid images, and tie points from the epipolar images were identified. In order to further refine the tie points, aerial based matching was again conducted using the next pyramid level. This procedure was applied iteratively until the most accurate pyramid layer was used. A subset of points was obtained and interpolated by Kriging to generate a DEM. Blunders and incorrect matches were removed and a final DEM with a ground resolution of 20 m was obtained. Fig. 9 presents the shadow relief maps of the SRTM DEM and the SPOT derived DEM. Although the two shadow relief maps (Fig. 9(a) and (b)) look similar, the resolution and level of topographic detail of the SPOT derived DEM (Fig. 9(d)) are superior to those of the SRTM DEM (Fig. 9(c)). More detailed components of the DEMs are compared in the grey scale maps of Fig. 9(c) and (d).

5. Conclusions

ERS SAR data and the SRTM DEM may be used to obtain GCPs for georeferencing SPOT stereo pairs in locales where field surveyed data and published maps are not available. In this study, the ground coordinates of GCP candidates were calculated from ERS SAR data and the SRTM DEM. To effectively select only qualified GCPs from an initially extracted set of GCPs, we proposed and tested a method for eliminating unqualified GCPs based on residual errors of iterative orientation modeling. A total of 41 GCP candidates were obtained for the verification test. Positional errors of these GCPs were too large for direct application to the SPOT stereo pair. The GCP candidates satisfied two conditions: i) they had a Gaussian distribution and ii) there existed a linear relationship between the positional and residual errors. Through repeated orientation modeling, 20 GCPs were finally selected. The mean positional errors of the selected GCPs were 6.7 m, 7.6 m and -3.7 m in X-, Y- and Z-directions, respectively. Orientation modeling of the SPOT stereo pair was greatly improved by using only the finally selected 20 GCPs. RMSEs estimated from 15 check points were 10.4 m, 7.1 m, and 12.1 m in X, Y and Z directions, respectively. The final 20 GCPs were accurate enough to rectify a SPOT stereo pair and create a SPOT derived DEM with a ground resolution of 20 m. Thus, it is shown that a reliable DEM may be constructed using ERS SAR data, the SRTM DEM, and a SPOT stereo pair in areas where ground reference data is not available.

Acknowledgement

This work was funded by Korea Aerospace Research Institute within the framework of Development of KOMPSAT-5 system. We thank to anonymous reviewers for useful comments.

References

Chen, L. C. and J. Y. Rau, 1993. A unified solution for digital terrain model and orthoimage generation from SPOT stereopairs. *IEEE Transactions on Geoscience and Remote Sensing*, 31(6): 1243-1252.

Curlander, J. C. and R. N. McDough, 1991. *Synthetic*

Aperture Radar, Systems and Signal Processing, John Wiley & Sons, New York.

Dare, P. and I. Dowman, 2001. An improved model for automatic feature-based registration of SAR and SPOT images. *ISPRS Journal of Photogrammetry and Remote Sensing*, 56(1): 13-28.

Hong, S. H., H. S. Jung and J. S. Won, 2006. Extraction of ground control points (GCPs) from synthetic aperture radar image and SRTM DEM. *International Journal of Remote Sensing*, 27(18): 3813-3829.

Lee, H. S. and N. H. Younan, 2003. DTM extraction of lidar returns via adaptive processing. *IEEE Transactions on Geoscience and Remote Sensing*, 41(1): 2063-2069.

Lopes, A., E. Nezry, R. Touzi, and H. Laur, 1993. Structure detection and statistical adaptive speckle filtering in SAR images. *International Journal of Remote Sensing*, 14(9): 1735-1758.

Marschalk, U., A. Roth, M. Eineder and S. Suchandt, 2004. Comparison of DEMs derived from SRTM/X- and C-Band. *Proceedings of International Geoscience and Remote Sensing Symposium*, 20-24 September 2004, Anchorage, Alaska, USA, pp. 4531-4534.

Mikhail, E. M., J. S. Bethel, and J. C. McGlone, 2001. *Introduction to Modern Photogrammetry*, John Wiley & Sons, New York.

Olmsted, C., 1993. Alaska SAR Facility Scientific SAR User's Guide, ASF-SD-478.

Orun, A. B. and K. Natarajan, 1994. A modified bundle adjustment software for SPOT imagery and photography: Tradeoff. *Photogrammetric Engineering and Remote Sensing*, 60(12): 1431-1437.

Paul, D. and I. Dowman, 2001. An improved model for automatic feature-based registration of SAR and SPOT images. *ISPRS Journal of Photogrammetry and Remote Sensing*, 56(1): 13-28.

Rabus, B., M. Eineder, A. Roth and R. Bamler, 2003. The shuttle radar topography mission:a new class of digital elevation models acquired by spaceborne radar. *ISPRS Journal of Photogrammetry and Remote Sensing*, 57(4): 241-262.

Raucoules, D. and C. Carnec, 1999. Use of interferometric phase for co-registration of ERS SAR and SPOT images. *Proceeding of CEOS SAR Workshop*, 26-29 October 1999, Toulouse, France, pp.114-118.

Raillou, P. and M. Gelautz, 1999. Relief reconstruction from SAR stereo pairs: the "optimal gradient" matching method. *IEEE Transactions on Geoscience and Remote Sensing*, 37(4): 2099-2107.

Rufino, G., A. Moccia and S. Esposito, 1998. DEM generation by means of ERS tandem data. *IEEE Transactions on Geoscience and Remote Sensing*, 36(6): 1905-1912.

Shapiro, S. S. and M. B. Wilk, 1965. An analysis of variance test for normality complete samples. *Biometrika*, 52: 591-611.

Toutin, T., 2000. Stereo-mapping with SPOT-P and ERS-1 SAR images. *International Journal of Remote Sensing*, 21(8):1657-1674.

Toutin, T., D. Hoja, E. Hoeppner, A. Remond, and C. King, 1998. GCPs Selection from Multi-source Data Over Mountainous Topography. *Proceeding of International Geoscience and Remote Sensing Symposium*, 6-10 July 1998, Seattle, USA, pp.2339-2341.